

1 **Uncertainties in temperature statistics and fluxes determined by**  
2 **sonic anemometer due to wind-induced vibrations of mounting arms**

3 Zhongming Gao<sup>1,2,3</sup>, Heping Liu<sup>3,\*</sup>, Dan Li<sup>4</sup>, Bai Yang<sup>5</sup>, Von Walden<sup>3</sup>, Lei Li<sup>1,2</sup>, Ivan Bogoev<sup>5</sup>

4  
5 <sup>1</sup> School of Atmospheric Sciences, Sun Yat-sen University, Southern Marine Science and Engineering  
6 Guangdong Laboratory (Zhuhai), Zhuhai, China

7 <sup>2</sup> Key Laboratory of Tropical Atmosphere-Ocean System, Ministry of Education, Sun Yat-sen University,  
8 Zhuhai, Guangdong, China

9 <sup>3</sup> Laboratory for Atmospheric Research, Department of Civil and Environmental Engineering,  
10 Washington State University, Pullman, Washington, USA

11 <sup>4</sup> Department of Earth and Environment, Boston University, Boston, Massachusetts, USA

12 <sup>5</sup> Campbell Scientific, Inc., Logan, Utah, USA

13

14 **Corresponding author:** Heping Liu ([heping.liu@wsu.edu](mailto:heping.liu@wsu.edu))

15

16 **Contents of this file:**

17 Text S1 to S2

18 Figures S1 to S2

19 Tables S1 to S2

20

21 **Text S1. Investigation of the impact of solar heating on  $T_s$  and  $T_c$  spectra**

22 To investigate the potential impacts of solar heating on the difference of  $T_s$  and  $T_c$   
23 spectra, we examined two sets of data, one from nighttime and one from daytime, with similar  
24 wind speeds and wind directions (i.e.,  $7 \text{ ms}^{-1} < \bar{u} < 9 \text{ ms}^{-1}$ ;  $40 \text{ deg} < \text{WD} < 80 \text{ deg}$ ). The average  
25 normalized power spectra and cospectra were calculated as a function of natural frequency ( $f$ )  
26 (Figure A1). Both at night ( $n = 26$ ) and during the day ( $n = 9$ ), it was observed that the power of  
27  $T_s$  spectra was higher in the high frequency range and lower in the low frequency range than  $T_c$ .  
28 This aligns with the findings in the main text, suggesting that the difference between  $T_s$  and  $T_c$   
29 spectra was likely not due to solar heating effects on the fine-wire thermocouples. Here  $n$  is the  
30 number of selected 30-min time series in each group.

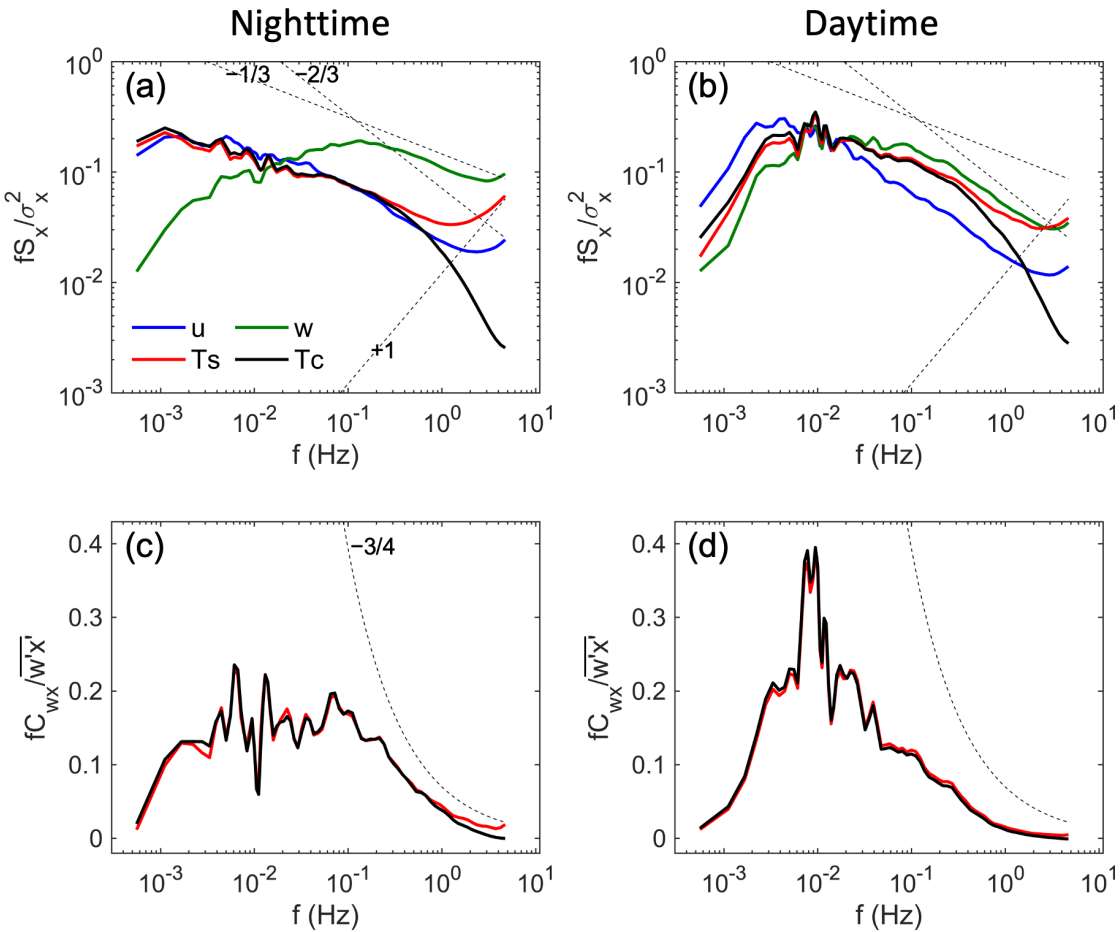
31  
32

33 **Text S2. Investigation of the impacts of wind speed on the spectra distortion in the high frequency**  
34 **range**

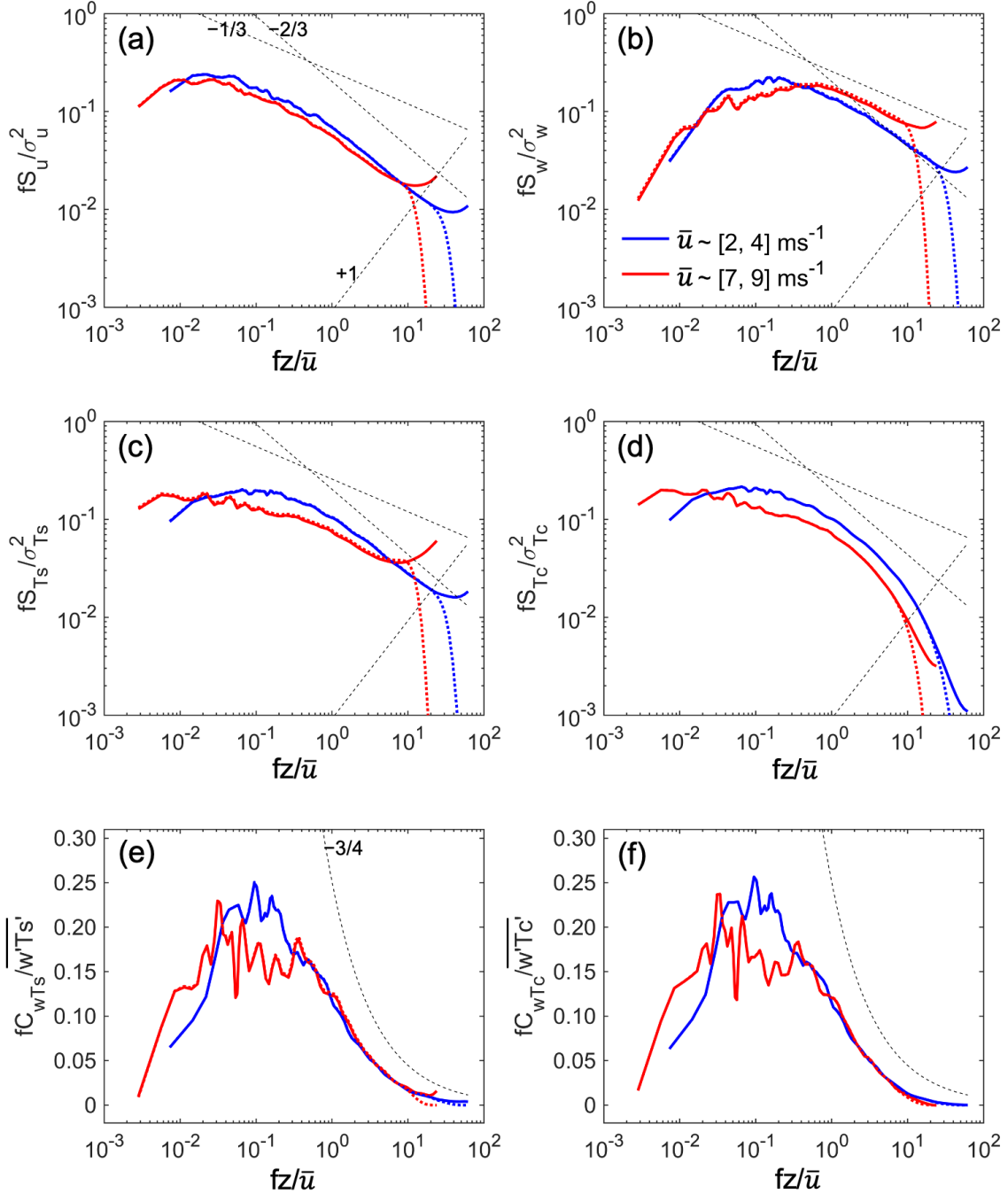
35 To investigate the potential causes for the spectral distortion in the high frequency range  
36 (i.e.,  $f > 0.2 \text{ Hz}$ ), we selected two sets of data with similar wind directions but different wind  
37 speeds. We then calculated the average normalized power spectra and cospectra as a function of  
38 nondimensional frequency ( $fz/\bar{u}$ , where  $z$  is the measurement height,  $\bar{u}$  is the mean wind speed;  
39 Figure S2). For instance, at the height of 40.2 m, all power spectra of  $u$ ,  $w$ , and  $T_s$  illustrated a  
40 upturned distortion at the high frequency end (e.g.,  $fz/\bar{u} > 5$ ) due to white noise. Under low  
41 wind conditions (i.e.,  $2 \text{ ms}^{-1} < \bar{u} < 4 \text{ ms}^{-1}$ ;  $40 \text{ deg} < \text{WD} < 80 \text{ deg}$ ;  $n = 126$ ), the power spectra  
42 generally followed the  $-5/3$  power law. However, under high wind conditions (i.e.,  $7 \text{ ms}^{-1} < \bar{u} <$   
43  $9 \text{ ms}^{-1}$ ;  $40 \text{ deg} < \text{WD} < 80 \text{ deg}$ ;  $n = 70$ ), both the  $w$  and  $T_s$  spectra were significantly distorted,  
44 following a  $-4/3$  power law for approximately  $0.5 < fz/\bar{u} < 5$ . This suggests that the upturned  
45 distortion in the  $T_s$  spectra was linked to increasing wind speed. For the power spectra for  $T_c$ ,  
46 both groups showed similar declining trends in the high frequency range, indicating that the FW3  
47 was not affected by increased wind speed.

48 As for the cospectra of  $w-T_s$  and  $w-T_c$ , they were nearly identical in the high-frequency  
49 range (i.e.,  $fz/\bar{u} > 1$ ). This indicates that the above-mentioned distortion in the  $w$ ,  $T_s$ , and  $T_c$   
50 spectra had no significant influence on the mean normalized cospectra. Overall, these results  
51 suggest that more high-frequency noises/spikes were induced to the time series of  $T_s$  with the

52 increasing wind speeds. While this affected the corresponding spectra somewhat, it had no  
 53 significant impact on the cospectra. Different tests, where we excluded the first EEMD  
 54 component with the highest frequency, showed that the spectral distortion in the  $u$ ,  $w$ , and  $T_s$   
 55 spectra was largely eliminated (dotted lines in Figures S2). This contributed approximately 1–2%  
 56 to the corresponding variances. Again, the impact on the corresponding cospectra was minor.  
 57  
 58



59  
 60 **Figure S1.** Mean normalized power spectra of  $u$ ,  $w$ ,  $T_s$ , and  $T_c$  and cospectra of the  $w-T_s$  and  $w-T_c$  for  
 61 two groups data under the nighttime and daytime conditions with the same wind speed range ( $7 \text{ ms}^{-1} < \bar{u}$   
 62  $< 9 \text{ ms}^{-1}$ ) and wind direction range ( $40 < \text{WD} < 80$  degree) at the height of 40.2 m. The dashed lines show  
 63 a  $f^{-1/3}$ ,  $f^{-2/3}$ ,  $f^{-3/4}$ , and  $f^{+1}$  slope.  
 64  
 65



66

67 **Figure S2.** Mean normalized power spectra of  $u$ ,  $w$ ,  $T_s$ , and  $T_c$  and cospectra of the  $w-T_s$  and  $w-T_c$  for  
 68 two groups data with different wind speeds but similar wind directions ( $40 < \text{WD} < 80$  degree) at the  
 69 height of 40.2 m. The dotted color lines are the corresponding spectra and cospectra after removing the  
 70 first EEMD component. The dashed lines show a  $f^{-1/3}$ ,  $f^{-2/3}$ ,  $f^{-3/4}$ , and  $f^{+1}$  slope.

71

72

73

74

75 **Table S1.** Contributions of the three regimes to the total variances and fluxes of water vapor  
 76 density corrected by  $T_s$  and  $T_c$ .  $\rho'_{v,y}$  refers to the fluctuations of water vapor density corrected by  
 77 temperature  $y$  (i.e.,  $T_s$  and  $T_c$ ) using equations (2).

		40.2 m	23.0 m	12.8 m
$\sigma_{\rho_{v,T_s},i}^2 / \sigma_{\rho_{v,T_s}}^2$	I	0.76	0.76	0.68
	II	0.18	0.17	0.17
	III	0.06	0.06	0.15
$\sigma_{\rho_{v,T_c},i}^2 / \sigma_{\rho_{v,T_c}}^2$	I	0.76	0.77	0.68
	II	0.18	0.17	0.17
	III	0.06	0.06	0.15
$\overline{w' \rho'_{v,T_s,i}} / \overline{w' \rho'_{v,T_s}}$	I	0.64	0.47	0.34
	II	0.31	0.35	0.48
	III	0.04	0.13	0.17
$\overline{w' \rho'_{v,T_c,i}} / \overline{w' \rho'_{v,T_c}}$	I	0.64	0.48	0.35
	II	0.31	0.36	0.48
	III	0.04	0.13	0.16

78

79

80

81

82

83

84

85

86

87

88

89

90

91 **Table S2.** Contributions of the three regimes to the total variances and fluxes of CO<sub>2</sub> concentration  
 92 corrected by  $T_s$  and  $T_c$ .  $\rho'_{c,y}$  refers to the fluctuations of CO<sub>2</sub> concentration corrected by  
 93 temperature  $y$  (i.e.,  $T_s$  and  $T_c$ ) using equations (3).

		40.2 m	23.0 m	12.8 m
$\sigma_{\rho_{c,T_s,i}}^2 / \sigma_{\rho_{c,T_s}}^2$	I	0.39	0.48	0.26
	II	0.29	0.15	0.23
	III	0.32	0.37	0.51
$\sigma_{\rho_{c,T_c,i}}^2 / \sigma_{\rho_{c,T_c}}^2$	I	0.40	0.47	0.28
	II	0.31	0.15	0.25
	III	0.29	0.38	0.48
$\overline{w'\rho'_{c,T_s,i}} / \overline{w'\rho'_{c,T_s}}$	I	0.62	0.44	0.09
	II	0.25	0.44	0.26
	III	0.03	0.11	0.57
$\overline{w'\rho'_{c,T_c,i}} / \overline{w'\rho'_{c,T_c}}$	I	0.55	0.37	0.19
	II	0.25	0.40	0.32
	III	0.11	0.20	0.43

94

95